Rev. Adv. Mater. Sci. 40 (2015) 262-275

ATOMIC LAYER DEPOSITION OF TIN DIOXIDE NANOFILMS: A REVIEW

D.V. Nazarov, N.P. Bobrysheva, O.M. Osmolovskaya, M.G. Osmolovsky and V.M. Smirnov

Saint-Petersburg State University, Institute of Chemistry, Universitetskii pr. 26, Petrodvoretz, Saint Petersburg, 198504, Russia

Received: October 20, 2014

Abstract. Due to unique electrical, optical, chemical and magnetic properties of tin dioxide, SnO_2 thin films attract enormous attention as a potential material for gas sensor devices, transparent conducting oxides for microelectronics, lithium-ion batteries, supercapasitors, spintronic devices, solar cells, etc. Thin films possessing a wide variety of properties determined by thickness, morphology, structural properties, and film composition are necessary to satisfy the requirements of such a wide range of applications. At present, there are many approaches for SnO_2 thin films manufacturing, the Atomic Layer Deposition (ALD) technology is considered to be the most promising and suitable method to produce thin film with a set of certain characteristics. In this paper, we present an overview of achievements in SnO_2 ALD thin film preparation. The special attention is given to the selection of precursors, deposition conditions, and deposited films properties.

1. INTRODUCTION

Tin dioxide, SnO_2, is a wide band-gap semiconductor material with excellent optical, electrical, magnetic, and chemical properties [1-3]. As a consequence, SnO_2 is used in a variety of applications. This oxide is the most interesting and promising material for solid state gas sensor devices [1,2,4-8]. Sensing mechanism is based on band bending induced by adsorption of charged molecules which cause the increase or decrease in surface conductivity [1,5]. The dual valence of tin facilitates a reversible transformation on the surface of this oxide enabling to use this compound as an oxidation catalyst [1,9-11].

High transmittance in the visible region of the spectrum and relatively high electrical conductivity determine the using of tin oxide as transparent conducting oxides (so called TCOs) [1,12,13]. Solid solution of indium tin oxide (ITO) is one of the most commercially important TCOs [12-15], but in recent years zinc tin oxide (ZTO) has become increasingly important because of its lower cost and scarcity [16]. TCOs are used in numerous technologies including field effect transistors for flexible displays [17-19], organic light-emitting diodes (OLEDs) [20-22] and solar cells [23-26]. Reflectance in infra-red (IR) permits to apply SnO_2 as surface coatings for functional glasses [27]. Tin oxide based materials having high specific surface area and conductivity are widely used in dye-sensitized solar cells. In such applications SnO_2 can be used instead of well known TiO_2 [28-30] or together with this oxide [31,32].

Among all metal oxides, tin dioxide is regarded as a promising candidate for anodic material for lithium-ion batteries because of its high reversible capacity and stability [33]. SnO_2 has also attracted considerable interest in the field of supercapacitors due to the non-toxic nature and low cost by com-

Corresponding author: D.V. Nazarov, e-mail: dennazar1@yandex.ru

parison to the most suitable RuO_2 [34-36]. There are a lot of works connected with the application of this oxide for wastewater treatment processes [37,38] and obtaining of nanometer-sized termite particles with greatly enhanced contact of fuel and oxidizer [39,40]. SnO_2 doped by 3d-elements exhibits ferromagnetic properties and can be used for the new generation of spintronic devices [41-45].

For such a variety of applications, the nanoobjects based on SnO_2 with different dimensions, composition, structure, and morphology are necessary. As a consequence, a number of methods are used for the tin dioxide preparation. 0-d nanoobjects (nanoparticles) are commonly obtained by sol-gel (precipitation) [46-48] or hydrothermal [49-52] methods. 1-d nanostructures (nanorods, nanobelts, nanowires, nanoneedles) can be produced by hydrothermal [5,51-53], chemical vapor deposition (CVD) [5,53-55], and some other methods [2,3,5,53]. 2-d nanomaterials (nanofilms and nanolayers) are obtained by spray-pyrolysis [56-58], spin-coating [59-61], physical vapour deposition (PVD) [58,62,63], sputtering [17,64,65], CVD [58,66-69], successive ionic layer deposition (SILD) [70,71] or atomic layer deposition (ALD) [6-8,16,18,19,36,39,40,72-98].

Despite the fact that sol-gel, various PVD and CVD technologies are extremely widespread in the production of thin film, ALD technique is more promising for the deposition of high quality and ultrathin films and coating because this method allows the formation of the material in an atomically controlled fashion on the surface of planar, three-dimensional and even the porous substrates [16,99,100]. The deposition of films by ALD method relies on successive, separated, self-saturating, and self-terminating gas–solid reactions (chemisorption) [100-102]. Simple metal-oxide ALD process consists of sequential proceeding of individual gas-surface reactions (half-reactions) of metal-containing and oxygen-containing (oxidizer) reactant with the substrate. H_2O is usually used as oxidizer but O_2, O_3, and H_2O_2 can be applied to increase the reactivity of chemisorbed element-containing reactants in the series of ALD processes. In the interval between the half-reactions the reactor is purged (purge stage) to remove reaction by-products and unreacted reagents. A single sequence of treatment and a purge stages is called a ALD cycle.

It's important to mention that the control of the film thickness at Angstrom level can be fulfilled by regulating a number of cycles. Precise control of the films composition can be carried out by the use of "super cycles", which are composed of several ALD cycles with various precursors [16,99]. It should be noted that the concept of so called "ALD-window" is extremely important for the ALD technology. ALD-window is a set of conditions when the growth rate per cycle (GPC) is constant, equal to mono or submonolayer and defined by the properties of surface and the chemisorption ability of the reactants. The main condition is temperature as well as pulse time, purge time, etc. A deviation from the ALD-window can lead to decrease of GPC due to incomplete chemisorption or reevaporation of chemisorbed precursors or increase because of thermal decomposition or physisorption process.

ALD are widely used for producing of different oxides such as Al_2O_3 [103-105], TiO_2 [106-108], ZnO [109-111], ZrO_2 [112-114], SiO_2 [115-117], VO_2 [118-121], as well as sulfides [122-124], selenides [125,126], nitrides [127-130], and various metal films [130-133]. For a more comprehensive summary of ALD technology and its variety of applications the reader is referred to existing reviews on the topic [16,99-102,134-138].

This review is intended to introduce the reader to advances in the obtaining of SnO_2 thin films by using ALD on different flat substrates with various precursors and terms of deposition, as well as to demonstrate the influence of different precursors, supports and conditions of synthesis on their composition and structure, defining a great variety of their properties.

2. DEPOSITION OF SnO_2 THIN FILMS USING INORGANIC REAGENTS

The most commonly used inorganic reagents for deposition of SnO_2 by ALD are $SnCl_4$ and SnI_4, see Table 1.

The first studies of SnO_2 nanofilms production using ALE (the original name for the ALD method) were performed by H. Viirola and L. Niinisto [72-77]. Tin oxide thick films (50-420 nm) were deposited on glass and silicon substrates using $SnCl_4$ and H_2O as reactants in the temperature range of 300-600 °C. It was discovered that ALD window was within 500-550 °C and the growth rate was about 0.35 Å per cycle [72]. In the following study these authors increased the GPC value to 0.6 Å by increasing of H_2O dose [74]. The films obtained at temperatures above 500 °C were polycrystalline and their crystallites had a preferred orientation which depended on the growth temperature and film thickness [72]. Heteroepitaxial SnO_2 films were also produced on the sapphire ($1\underline{1}02$) support [77].

Similar results were obtained by Hsyi-En Cheng et al. [78]. The growth rates were around 0.2, 0.4,

Table 1. ALD deposition of tin oxide using inorganic precursors.

Reagent 1 (Sn-containing)	Reagent 2 (oxidizer)	Substrate	Temperature, °C	Growth per cycle, Å	Structure/ Stoichiometry (Sn/O)	Ref.
$SnCl_4$	H_2O	Monocrystal silicon,	430-545	0.35-0.4	-	75
$SnCl_4$	H_2O	Soda lime glass	500	0.35	Polycrystalline stoichiometric	72
		Coming 7059 glass	300	0.14/0.11*	-	
$SnCl_4$	H_2O	Si (100), glass	300	0.21	Amorphous	78
			350	0.38	Polycrystalline	
			400	0.58	Polycrystalline	
			450	0.52	Polycrystalline	
$SnCl_4$	H_2O	SiGaAs	180	0.04	Amorphous/1.76	79
			300	0.17	Polycrystalline /1.92	
$SnCl_4$	H_2O	Soda lime glass	500	0.6	Polycrystalline /1.6-1.8	74
	H_2O+O_3		500	0.75	-	
	O_2		500	0	-	
$SnCl_4$	H_2O_2	αAl_2O_3- (012)	300	0.4	Polycrystalline	6,83,
			600	0.3	Polycrystalline	86
			700	-	Epitaxial	
$SnCl_4$	H_2O_2	Quartz, Si(100)	325	0.7	Amorphous /1.4-1.5	81
SnI_4	O_2	αAl_2O_3- (012)	400	≈0	-	84,85,
			500	1.0	Low-grade epitaxial	87
			600	1.1	Epitaxial	
			750	1.2	Epitaxial	
SnI_4	O_2	Si/SiO_2 (100)	400	0.4	Polycrystalline	85
			600	1.5	-	
			750	2.4	-	
SnI_4	H_2O_2	αAl_2O_3- (012)	100-200	0.65	Amorphous	87
			200	0.65	Polycrystalline	
			300	0.25	Epitaxial	
			400	0.2	Epitaxial	

* - growth per cycle depends on support type highlighted in terms of falling into the “ALD window”

0.6, and 0.5 Å per cycle for films grown at 300, 350, 400, and 450 °C, respectively. The films produced at temperatures above 350 °C were polycrystalline.

A.Tarre, A. Rosental, and J. Sundqvist obtained amorphous and amorphous with small amount of rutile-type SnO_2 polycrystalline layers at 180 and 300 °C respectively [79,80]. Growth rate per cycle was extremely low and amounted to 0.04 Å at 180 °C and 0.17 Å at 300 °C. The samples had a relatively smooth surface with estimated root-mean-square (RMS) equal to 0.32 nm for 8 nm films [79,80]. However, the roughness of the layers increased with the deposition growth temperature and film thickness [74,79,80]. Thus, the RMS was 3.6-8.2 nm for 90-140 nm thick films produced at 500 °C [74].

It should be noted that the films were nonstoichiometric with Sn/O ratio ranges from 1.76 to 1.92 [79,80] and from 1.6 to 1.8 [74]. Chlorine content was decreased as the temperature growth. It was about 8-9% for 180 °C [79], 3.6% at 500 °C

[74], and became below than the detection limits at temperatures above 500 °C [72].

Considering SnO_2 manufacturing from $SnCl_4$ and H_2O, the influence of gas-phase additives (n-hexane, ozone) and carrier gases (nitrogen, oxygen) on film growth and its properties should be taken into account [74]. The use of ozone together with H_2O increases the SnO_2 growth rate up to 0.74 Å at 500 °C. This behavior is associated with ozone-assisted H_2O dissociation that forms a high concentration of OH groups on the surface. Application of n-hexane gas-phase additive (hexane was pulsed after H_2O) slightly diminishes growth rate, increases resistivity, enhances crystallinity, and improves stoichiometry. Such changing of film characteristics is believed to take place due to a hexane-promoted reaction mechanism which can lead to enhanced water incorporation which forms and stabilizes oxygen ions into the lattice as evidenced by XRD and AFM data. The experiments carried out with O_2 carrier gas without the water pulse did not result in any film growth. Thus, the use of O_2 as a gas carrier does not contribute significantly to the SnO_2 layer growth [74].

Conductivities of films produced with various gas-phase additives and carrier gases differ significantly. Notably, the researchers supposed that the changes were caused by variation of carrier concentration due to different number of oxygen vacancies. The growth of oxygen content increases sample resistivity, while a relatively high chlorine content strongly decreases this characteristic [74].

X. Du and S. M. George carried out a detailed study of SnO_2 growth mechanism with application of $SnCl_4$ and H_2O_2 as oxidizer [81,82]. In situ quartz crystal microbalance (QCM) and Fourier transform infrared techniques (FTIR) were used for this purpose. This can prove that chloride chemosorption with $SnCl_4/H_2O_2$ as precursors is carried out with hydroxyl groups formed after peroxide application. QCM measurements were consistent with a tin oxide ALD growth rate of 0.7 Å at 325 °C. This growth rate is higher than 0.4 Å per cycle estimated by A. Tarre et al. [83]. According to Auger electron spectroscopy (AES), a small chlorine content (1.6%) was detected on the surface, but X-ray photoelectron spectroscopy (XPS) did not detect any chlorine after upper layer sputtering. X-ray diffraction (XRD) and XPS studies also revealed that films were amorphous and nonstoichiometric with Sn/O ratio of 1.4-1.5.

A. Tarre, A. Rosental, and J. Sudqvist carried also a series of studies of SnO_2 production from $SnCl_4$ and SnI_4 with application of different oxidising agents (H_2O, H_2O_2, O_2). $SnCl_4/H_2O_2$ and SnI_4/O_2 pairs of precursors were used to prepare epitaxial SnO_2 thin films on (012) oriented α-Al_2O_3 substrates [83-85]. The study of temperature dependence of growth rate revealed that GPC was practically equal to its maximum value within a wide temperature range. ALD window extended from 250 °C to 500 °C in the case $SnCl_4/H_2O_2$ and from 500 °C to 750 °C in the case SnI_4/O_2. The value of GPC for $SnCl_4/H_2O_2$ at 300 °C was 0.4 Å and 0.3 Å at 600 °C, the latter is similar to pair $SnCl_4/H_2O$ values [76] at 550 °C. It is explained probably by the fact that the peroxide is decomposed at such high temperatures and formed O_2 does not influence the SnO_2 growth [74]. The films obtained from SnI_4/O_2 had much higher GPC (1.1 Å) and remarkable smoothness. AFM data revealed that the films growth appears to be essentially two-dimensional in the beginning of the process and then becomes three-dimensional. For the both pairs of precursors the films were highly textured with preferential (101) orientation and a less marked (202) reflex.

The films, grown with using of $SnCl_4/H_2O_2$ at temperatures above 200 °C were crystalline. The increasing of film thickness worsens the crystallinity. The films grown at 700 °C in case of $SnCl_4/H_2O_2$ and above 400 °C in case of SnI_4/O_2 can be considered as epitaxial. The highest degree of epitaxy was obtained in case SnI_4/O_2 at 700 °C.

The comparison of SnI_4/O_2 films growth on different supports (oriented (012) α-Al_2O_3 and (100) Si/SiO_2) are presented in the study [85]. The growth rate on silicon support showed an almost linear increase from 0.4 Å at 400 °C up to 2.4 Å at 750 °C, that is, opposite to Al_2O_3 support there is no a plateau (ALD window) in this case. It can also be seen that the growth rate on Si/SiO_2 (100) substrates was faster at all except for the lowest temperatures. It is worth mentioning that no iodine could be detected by X-ray fluorescence spectroscopy and Rutherford backscattering spectroscopy (RBS) in any deposited films throughout the investigated temperature range. The ratio between Sn and O concentrations agrees with that of stoichiometric SnO_2.

A microstructure of epitaxial SnO_2 thin films obtained by ALD method on a-Al_2O_3 (012) substrates at 600 °C using $SnCl_4$ or SnI_4 was studied in [86]. It was found that the film/substrate interface was flat, clear, and did not contain any visible additional phase, while the film surface morphology and structure depend on the type of metal precursor.

Using of $SnCl_4$ leads to the formation of films with a rough surface and a high density of defects, including (011) and (101) twins and anti-phase boundaries (APBs). In contrast, the films from SnI_4

have uniform thickness, flat surface, and low density of APBs approach the perfect single crystal [86]. The data on the formation of SnO_2 films with using of SnI_4/H_2O_2 are also firstly presented in this paper. No significant difference in the structure and morphology of films has been found between the samples produced with O_2 and H_2O_2 precursors except for the film thickness.

The detailed comparison of the temperature dependence of growth rate for SnI_4/H_2O_2 and SnI_4/O_2 was demonstrated in [87]. While the growth from SnI_4/H_2O_2 takes place already at the lowest temperature applied (100 °C), the growth from the latter pair is lacking up to 400 °C. ALD windows are 100-250 °C (GPC – 0.65 Å) for SnI_4—H_2O_2 and 600-750 °C (GPC – 0.8-0.85 Å) for SnI_4—O_2. Low GPC for H_2O_2 at temperatures above 250 °C can be attributed to decomposition of H_2O_2 into nonreactive H_2O. The inactivity of H_2O in conjunction with SnI_4 follows from equilibrium thermodynamics and experimental study of this process. It should be noted that the crystallization starts above 200 °C for H_2O_2 and above 500 °C for O_2.

Thus, the reaction mechanism in these two cases cannot be identical. It is commonly accepted that the formation of oxide films from metal halides and oxygen-hydrogen compounds at low temperatures is provided by the halide precursor which connect with the surface via hydroxyl groups [138]. At higher temperatures and/or hydrogen-free oxidizing precursors like oxygen or ozone, the growth process is more complicated and other surface groups can be active.

To sum up, the use of $SnCl_4$ gives rise to not very high growth rate even in ALD window, significant contamination of the films by chlorine, high nonstoichiometry, and detectable amount of structure defects as well as large roughness owing to etching of the deposit by produced HCl [85]. For SnI_4, the above-listed parameters are better than for $SnCl_4$. The only advantages of tin chloride are low cost and availability.

SnI_4/H_2O_2 is the best suited pair for the low temperature process, SnI_4/O_2 pair - for high temperature process. The most reasonable oxidant for $SnCl_4$ is H_2O since H_2O_2 decomposition is observed at the required synthesis temperatures, whereas O_2 does not influence on a process.

Regarding films crystallinity, the crystallization temperature onset and the quality of the crystal structure strongly depend on the precursor used and the type of substrates. Thus, crystallization starts at 200 °C with H_2O_2 oxidizer for both $SnCl_4$ and SnI_4, at 300-350 °C in the case $SnCl_4/H_2O$ pair, and at temperatures above 500 °C using a SnI_4/O_2 pair. SnI_4/O_2 pair should be used at deposition temperature of at least 600 °C in order to prepare high quality epitaxial films.

3. DEPOSITION OF SnO_2 THIN FILMS USING METALORGANIC REAGENTS

The necessity to increase the growth rate, decrease process temperature, eliminate corrosive by-products such as HCl, and improve the film quality has led to an active search of Sn-metalorganic ALD precursors. To date, a variety of precursors (Table 2) and obtained films with different composition, morphology, structure, optical, and electrical (Table 3) properties have been studied.

3.1. Tetrakis(dimethylamino)tin (TDMASn)

One of the most perspective precursors for SnO_2 obtaining by ALD method is tetrakis(dimethylamino) tin (TDMASn) (Fig. 1). There was a number of theoretical and experimental studies of the process of tin oxide growth using TDMASn and various type of oxidants such as H_2O [19,88-90], O_3 [88,91], and H_2O_2 [19,88].

J. Elam et al. were the first to use this precursor [88]. As the oxygen sources, they have tested H_2O, H_2O_2, and O_3 oxidants; it was discovered that H_2O_2 provides the highest SnO_2 growth rates. The studies showed that SnO_2 growth rate decreased steadily from 1.58 Å at 50 °C to 0.83 Å cycle at 325 °C with the plateau in the interval 100-200 °C in the case of H_2O_2. In authors opinion, the thermal decomposition of TDMASn takes place at temperatures above 325 °C leading to a non-selflimited film growth. However, according to DSC data, TDMASn thermal decomposition is at about 230 °C that also leads to increase of growth rate for cycle [19].

There is a contradictions connected with determination of TDMASn pulse time required for saturation [88,89]. The authors of [88] believe that the total saturation must be reached in the minimum in-

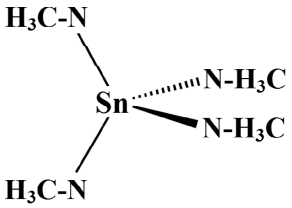

Fig. 1. Chemical formula of tetrakis (dimethylamino) tin.

Table 2. ALD deposition of tin oxide using metalorganic precursors.

Reagent 1 (Sn-containing)	Reagent 2 (oxidizer)	Substrate	Temperature, °C	Growth per cycle, Å	Structure/ Stoichiometry (Sn/O)	Ref.
TMT	NO_2	Si	400-450	2.5	-	98
TET			250-290	2.5		
TDMASn	H_2O	Si, glass	200	0.4	-	19
	H_2O_2		200	1.2	Amorphous	
			250		Polycrystalline/	
			100-250		2.27-2.08	
TDMASn	H_2O	Si (100),	30	2		89
		microscope slide glass	150	0.7	Amorphous	
TDMASn	H_2O_2 (50%)	Glass, Si (100)	100–200	1.2	Amorphous	88
			50–325	1.58-0.83		
TDMASn	O_3	Si, SiO_2, glass	50	1.6	Amorphous	91
			150	1.0	Amorphous	
			250	1.5	Polycrystalline/	
			100-200		1.8-1.9	
Sn(tbba)	H_2O_2 (50%)	Si/SiO_2 glass, SiN membrane	50-150	1.8	1.62-2.23*	95
			250	1.1	-	
			120	1.8	Polycrystalline	
Sn(tbba)	H_2O	Si/SiO_2	150	0.16	-	95
Sn(tbba)	NO	Silica glass	130	2.3	-	96
			170	1.9	-	
			200-250	1.4	Polycrystalline/	
			130-250		2.13-1.93	
$Sn(acac)_2$	O_3	Si (100)	175-300	1	-	97
			200	-	Amorphous/2.4	
			200-300	-	-	
		O_2	-	0	-	
		H_2O	-	0	-	
DBTA	O_2PEALD	Si (100)	200	0.8	Polycrystalline/	7
		SiO_2-130nm	300	0.9	1.6-2**	
			400	1.0		
DBTA	O_2PEALD	(110) (a-cut)(100) (m-cut)sapphire	300	1.1	Epitaxial/ Stoichiometric	92
DBTA	O_2PEALD	TiO_2 (100) (001) (110) (101)	300	0.9	Epitaxial/ stoichiometric	8
DBTA	O_2PEALD	YSZ (100)	300	0.6	Epitax.(C)***	93
		YSZ (110)			Epitax. (C)***	
		YSZ (111)			Polycrystalline/ Stoichiometric	
Tin(IV)-butoxide	O_2PEALD	Stainless steel	200	1	-	94
Sn $(dmamp)_2$	O_2PEALD	Si/SiO_2-200nm	70-100	-	Amorphous	18
			130	-	Polycrystalline /1.7±0.3	

* - depends on number H_2O_2 doses
** - depends on the number of cycles
*** - (C) Orthorhombic columbite structure
highlighted in terms of falling into the “ALD window”

Table 3. Electrical properties of the SnO_2-ALD films.

Reagent 1 (Sn-containing)	Reagent 2 (oxidizer)	Substrate	Temperature, °C	Resistivity Ohm*cm	Ref.
$SnCl_4$	H_2O	Soda lime glass Coming 7059 glass	500	0.06-0.20*	72
$SnCl_4$ H_2O	H_2O+O_3	Soda lime glass	500	2-89** 12	74
$SnCl_4$	H_2O	Si (100), glass	300 350 400 450	0.01 0.06 0.11 0.06	78
TMT	NO_2	Si	400 425 450	0.21 0.17 0.13	98
TET	NO_2	Si	250 290	0.027 0.012	98
$Sn(dmamp)_2$	PEALD	Si/SiO2-200nm	130 200	0.37 0.02	18
Sn(tbba)	H_2O_2 (50%)	Si/SiO_2, Glass SiN membrane	120 100-220	0.0133*** 0.015-0.025	95
Sn(tbba)	NO	Silica glass	250	0.008	96
$Sn(acac)_2$	O_3	$Si (100)/SiO_2$-100nm	200	0.6	97
TDMASn	H_2O H_2O_2	Si, glass	100 200	6 0.00097	19
TDMASn	O_3	Si, SiO_2, glass	125 200	273 0.000563	91
DBTA	O_2PEALD	YSZ (100) YSZ (110) YSZ (111)	300	0.02	93

* - depends on film thickness
** depends on gas-phase additives and carrier gas
*** - depends on number H_2O_2 doses

terval of 10 seconds because of dimethylamine produced during the deposition binds strongly to hydroxylated substrate and limits the further TDMASn adsorption for low pulse time. However, this effect was not observed in [89] study in which water was used as the counter-reactant and the saturation was reached during 1 second. Such contradiction can be explained by a particular reactor design and operating conditions of process. In spite of these contradictions, all authors agree that ALD window is in the interval 100-200 °C for TDMASn/H_2O_2 pair.

In situ quartz crystal microbalance (QCM) and quadrupole mass spectrometry (QMS) data reported in [88], gives the authors the opportunity to explain the difference between growth rate for various oxidants (H_2O and H_2O_2) and to suggest the following mechanism of process with H_2O_2 as oxidizer.

$$\equiv OHx + Sn(DMA)_4 \rightarrow \equiv (O)\,xSn(DMA)_{4-x} + xHDMA, \quad (1)$$

$$\equiv (O)\,xSn(DMA)_{4-x} + 2H_2O \rightarrow \equiv O_2Sn(OH)\,x + 4 - xHDMA + O_2\,. \quad (2)$$

In these equations, the ≡ represent the chemosorbed species, DMA is the dimethylamino ligand, HDMA is dimethylamine, and *x* is the number of DMA ligands released during the TDMASn exposures [88].

QCM and QMS measurement revealed that *x*=3.0-3.2 which indicates that, on average, 20-23% of the DMA ligands remain on the surface after reaction 1. For the pair TDMASn/H_2O *x* = 2.5 and 37% of the DMA ligands remain on the surface. With H_2O, the growth rate is equal to 0.6 Å, while using

H_2O_2 allows to achieve 1.3 Å/cycle. The point is that DMA ligands cause steric hindrance and inhibit TDMASn adsorption lowering the SnO_2 growth rate [88]. In case of TDMASn/H_2O precursors [89], the process mechanism is following:

$$\equiv OHx + Sn(DMA)_4 \rightarrow \equiv (O)\,xSn(DMA)_{4-x} + xHDMA, \quad (3)$$

$$\equiv (O)\,xSn(DMA)_{4-x} + 2H_2O \rightarrow \equiv (OH)_x + 4-xHDMA + SnO_2\,. \quad (4)$$

In spite of a higher growth rate for H_2O_2 in comparison to water at temperatures above 100 °C, the authors [89] demonstrated that TDMASn/H_2O pair allows production of tin oxide with very high growth rate at low temperatures since growth rate raises with the decreasing of temperature and becomes equal to 2.0 Å/cycle at 30 °C as compared to 0.70 Å/cycle at 150 °C. It should be noted that ALD process is established to be saturated even at the lowest temperature studied, for which the film contamination levels are below the detection limits of XPS [89]. This fact is in a contrast with the results of [88] where the sharp increase of carbon and nitrogen content was found at the temperatures below 100 °C by XPS data. Nevertheless, the increase in the growth rate at temperatures below 100 °C was clearly established by different authors for H_2O [19,88,89] as well as H_2O_2 [19,88].

The explanation of this phenomenon was given in [90] which presents results of density functional theory and second-order Møller-Plesset perturbation theory calculations of ALD process using TDMASn and H_2O. At temperatures below 100 °C, the films growth is determined by the process of water physisorption. The authors demonstrated that the energetics for the TDMASn reaction with surface OH groups are similar to that with H_2O molecules. As a consequence, TDMASn can react with physisorbed water as well as surface hydroxyl groups and the summary process can be considered as mixed CVD/ALD or "controlled" CVD. As it was also shown, the reaction barrier for the water half reaction depended on the presence of hydroxyl groups adjacent to $O_2SnN(CH_3)_2$* reaction sites on the growth surface, and this fact played an important role in tin oxide ALD at low deposition temperatures.

O_3 as an oxidant was used by different scientific groups [88,91]. In this variant of ALD process, the following particularities of growth rate temperature dependence were found. First, the growth rate decreased gradually with increasing of temperature in a range from 50 to 150 °C. Generally, this dependence could be originated from an incomplete chemical reaction [100]. Above 200 °C, the growth rate increased from 1.09 Å/cycle (200 °C) to 1.48 Å/cycle (250 °C). This tendency could be explained by thermal decomposition of TDMASn [19].

It was also found by authors [91] that the refractive index value increased gradually as temperature rises, and saturated above the temperature of 200 °C (2.03–2.05). At the low temperature range, the observed lower refractive index value explained by the incorporation of impurities in the films or physisorbed molecules or unreacted ligands on the surface. This suggestion is confirmed by XPS data. Carbon impurities were detected at 100 °C (4.04 at.%) and 150 °C (2.27 at.%), and then removed above 200 °C [91]. As temperature decrease, the increasing of impurities amount diminishes a carrier concentration and leads to conductivity decrease by 6 orders of magnitude at temperature growth from 150 to 200 °C. These results indicate that the production of pure and high conducting ALD SnO_2 thin film with using of TDMASn/O_3 requires the temperatures at least higher than 200 °C. Considering that there no clear and wide ALD window with using of O_3, the best process temperatures should be near 200 °C.

It is important that the use of all oxidants leads to obtaining of smooth films with RMS value near 1 nm which is close to value of substrate smoothness. The study of the crystal structure showed that the formation of amorphous films at low temperatures is typical without regard to the kind of oxidants. For H_2O, the films had amorphous structure at 50-300 °C [89]. In the case of ozone, polycrystalline samples are obtained at 250 °C [91]. In case of H_2O_2, a process of crystallization begins at 200 °C [19].

According to XPS analysis results, the obtained films are usually oxygen-deficient that is nonstoichiometric. In case of peroxide oxidizer, the Sn/O values are in the limits of 0.95-1.4 [88], in the case of O_3 – 1.8-1.9 [91] and in the case of water does not reach 2 (stoichiometric value) [89]. Taking into account that the depth of analysis by XPS method probes is several nanometers only, this measurements reflect an oxygen deficient SnO surface layer of the films. It is believed that the composition of all obtained films in most cases is stoichiometric or close to this value. Furthermore, the typical refractive index values of SnO_2 are close to 1.9-2.0 compared to 2.4 that is typical of SnO.

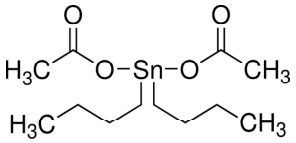

Fig. 2. Chemical formula of dibutyltindiacetate.

A conductivity of films without regard to oxidant type depends strongly on synthesis temperature and reaches maximum values near temperature range 200-250 °C [19,88,91]. They are $5.63*10^{-4}$ Ohm*ñm for O_3 [91] and $9.7*10^{-4}$ for H_2O_2 [19] (Table 3). There is also the dependence of conductivity on carrier concentration amounts which raises with the increasing of oxygen vacancies i.e. the growth of film nonstoichiometry.

3.2. Dibutyltindiacetate (DBTA)

The application of dibutyltindiacetate (DBTA) (Fig. 2) is limited by low reactivity of this reagent with standard ALD oxidants and therefore, a technology of ALD enhanced by oxygen plasma (PEALD) is used in this case. PEALD is a promising technique to produce high purity and high density metal oxide thin films at low growth temperatures [115,136,139].

G. Choi was first who demonstrated the possibility of practicable application of dibutyltindiacetate (DBTA) as a precursor for PEALD tin oxide [7]. Silicon substrate (100) was used as support. The growth rate was high and are in the range from 0.8 to 1.1 Å over temperature interval of 200-400 °C.

Dai Hong Kim et al. reported the series of successful experiments on obtaining of epitaxial stoichiometric SnO_2 films on various types of supports such as TiO_2 single crystal with orientations (100), (001), (110), (101) [8], (110) (a-cut), (100) (m-cut) sapphire [92] and (100), (110), (111) yttrium-stabilized zirconia (YSZ) substrates [93]. Polycrystalline films are obtained only in the case of (111) YSZ support, but in the other cases they are epitaxial. All films have a very strong preferred orientation normal to those of substrates. However, the additional weak (200) and (301) diffraction lines were found in the films deposited on a- and c-cut sapphire, respectively.

It is important to note that the films formed on YSZ substrate have the orthorhombic columbite structure that is not typical for SnO_2. Such modification was previously obtained by MOCVD and PLD methods under high pressure [140-142]. All YSZ-SnO_2 films exhibited the similar electrical resistivity of $2*10^{-2}$ Ohm*cm and the change of the electrical resistivity values with film orientation and phase was not significant.

3.3. Tin (IV)-butoxide

PEALD technology was successfully used for preparing performance SnO_2 anode for Li-ion batteries using tin (IV)-butoxide as precursor [94]. The films deposited on stainless steel substrate was amorphous and GPC was 1 Å at 200 °C.

3.4. N,N2-trimethyl-2-propoxy tin ($Sn(dmamp)_2$)

The tin oxide films were deposited onto quartz substrates and thermally grown SiO_2 (200 nm) on a highly phosphorous doped Si (001) by PEALD with aminoalkoxide precursor $Sn(dmamp)_2$ (Fig. 3) and oxygen plasma by B.K. Lee [18]. Substrate temperature ranged from 50 to 200 °C. On the one hand, tin oxide films deposited at 130 °C onto a quartz substrate had the rutile polycrystalline structure of SnO_2 and on the other, the films deposited at temperatures of 70 and 100 °C have an amorphous structure. Tin oxide films deposited at 70 and 130 °C were an insulator, but the carrier concentration above 130 °C increases drastically up to $10*19$ cm^{-3} at 200 °C and the resistivity diminishes down to $2*10^{-2}$ Ohm*cm (Table 3). The authors explain the increasing of conductivity with the process temperature growth and the transition of films from amorphous to crystalline state by decreasing of the amount of trapping sites of free carriers which concentrate on the grain boundaries.

XPS method showed that SnO_2 films do not contain any serious amounts of Sn^{2+}. But AES depth profile of a tin oxide film deposited at 130 °C revealed that the atomic ratio of tin to oxygen was estimated to be about 1:1.7±0.3, that points to an oxygen deficient environment and, as consequence, a possibility of n-type conductivity.

3.5. N2,N3-di-tert-butyl-butane-2,3-diamidotin(II) (Sn(tbba))

It is possible to use precursors containing Sn^{+2} for obtaining Sn^{+4} oxide films but this process does not necessarily require plasma treatment. J. Heo et al. carried out the low temperature ALD with the

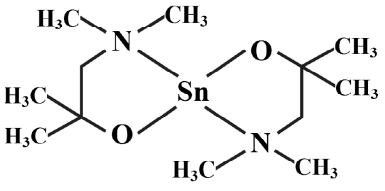

Fig. 3. Chemical formula of N,N2-trimethyl-2-propoxy tin.

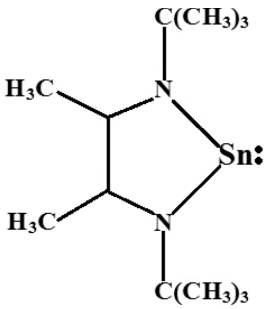

Fig. 4. Chemical formula of N2,N3-di-tert-butyl-butane-2,3-diamido tin (II).

using N2,N3-di-tert-butyl-butane-2,3-diamido tin (II) (Fig. 4) and H_2O_2 [95]. Due to the high reactivity of hydrogen peroxide with Sn precursor, the authors achieved high-purity and conducting tin oxide films at the deposition temperature as low as 50 °C. The ALD window was observed from 50 to 150 °C with GPC 1.7-1.8 Å. At temperatures above 150 °C, the growth rate of tin oxide decreased with the deposition temperature increase. It can be caused by the accelerated decomposition of H_2O_2 at high temperature and, as a consequence, the decrease in a number of surface hydroxyl groups, which subsequently act as adsorption sites for Sn precursors. When peroxide is substituted by water, the growth rate decreases to 0.16 Å (i.e. more than 10 times).

NO is also used as an oxidant gas [96]. Nitric oxide demonstrated the high reactivity toward the Sn(II) precursor and the growth rate was as high as 1.4 Å/cycle in 200-250 °C temperature range. At temperatures below 200 °C, the growth rate raised but the density of films measured by X-ray reflectivity (XRR) was significantly decreased and refractive index diverged considerably from typical for SnO_2. Lower film roughness was also observed for films grown at higher temperatures (230 and 250 °C). The RBS analysis showed the decreasing O/Sn ratio from 2.13 to 1.93 as the growth temperature increases from 130 to 250 °C. For H_2O_2 oxidizer, this ratio raises from 1.6 to 2.2 as the doses number (pulsing time) H_2O_2 increases [95]. The ratio Sn\O was also higher than two in the case of TDMASn/H_2O_2 using at low temperatures [19] and can be explained by the presence of unstable oxygen species such as hydroxyl groups, interstitial oxygen, or oxygen at grain boundaries which can be incorporated into the films at relatively low synthesis temperature.

The presence of unstable oxygen species affects significantly the conductivity. In the case of H_2O_2, lack in the films resistivity reaches values higher than 10^5 Ohm*cm [95]. The lowest resistivity - $1.33*10^{-2}$ Ohm*cm (Table 3) is observed for the films which composition is not stoichiometric but close to this value. In the case of NO, the factor which determined conductivity is the nitrogen content; nitrogen can trap free carriers here. The conductivity values drastically decrease with increasing growth temperature from 130 to 200 °C and then slowly decrease above 200°C. For NO, the lowest resistivity of $8*10^{-3}$ Ohm*cm was estimated (Table 3). However, high resistivity of the low temperature films may also come from their low density and refractive index.

It is noted that nitrogen contamination of the film is more likely appeared from the NO gas than from the ligand of the precursor. Otherwise, a large amount of carbon would accompany the nitrogen, however, this fact was not observed. What is more, the substantial amounts of nitrogen and carbon impurities for H_2O_2-SnO_2 films were not also detected.

It should be particularly emphasized that the films produced with H_2O_2 participation are polycrystalline even at 120 °C. NO-SnO_2 films are less crystallized. In the case of NO, the low crystallinity might be due to the presence of nitrogen in the film, that inhibits crystal growth. The ALD of crystalline SnO_2 films at a low temperature (130 °C) has been discussed previously for other Sn (II) precursor such as $Sn(dmamp)_2$ [18].

3.6. Acetylacetonate tin (II) ($Sn(acac)_2$)

Liquid tin(II) precursor, tin(II) acetylacetonate (Fig. 5) was used to deposit tin oxide films on Si(100) substrate [97]. Three different oxidizers such as water, oxygen, and ozone were tried. When employing ozone, the film growth rate was found to be 1±0.1 Å/cycle in the wide range of ALD window temperature from 175 to 300 °C and no film growth was observed with water or oxygen. The growth of reactivity of the precursor and ozone at higher temperatures elucidates formation of a dense film and, as a consequence, the increase in refractive index.

Carbon contamination (approx. 4 at.%) was detected even after 30 min of argon sputtering of the film, which is not uncommon for the films deposited using β-diketonate precursors [102]. The atomic ratio

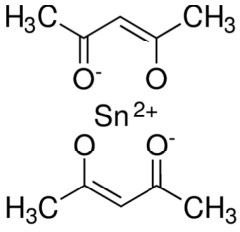

Fig. 5. Chemical formula of tin(II) acetylacetonate.

of O/Sn was found to be 2.4. The possible reasons of excess oxygen were discussed previously (part 3.5) but an additional factor can be carbon contamination. XPS study showed the formation of a clear SnO_2–Si interface. As-deposited tin oxide films were amorphous. The resistivity of the SnO_2 films was calculated to be 0.6 Ohm*cm. These results demonstrate the possibility of introducing $Sn(acac)_2$ as tin precursor to produce conducting ALD SnO_2 thin films with clear interface on a silicon surface without a formation of undesired SiO_2 or other interfacial reaction products for transparent conducting oxide applications.

3.7. Tetramethyl and tetraethyl tin ($SnMe_4$ and $SnEt_4$)

Among the metal-organic precursors which are used for SnO_2-ALD, it should be pointed out to liquid tetramethyl (TMT) and tetraethyl (TET) tin precursors. They have a reasonable vapor pressure and are in common use for CVD-SnO_2 deposition [68,69]. However, the application of strong oxidizers is necessarily for a common temperature of ALD process.

Drozd et al. [98] were the first to carry out ALD synthesis with these compounds and N_2O_4 as oxidizer. It was found that the ALD window for TMT and TET lies in the range of 400-450 °C and 250-290 °C respectively and GPC was 2.5 Å. A delay in the beginning of growth process was noted because of the difficulties of “active oxygen” formation in the upper layer of the substrate. It was shown that «active oxygen atom» can be produced by buffer oxide layers containing the elements with variable valence (Ti, Sn, Cr). This “atom” can reduce and transfer oxygen after stage (7) to tin atom oxidizing Sn(II) to Sn(IV).

$$Et_4Sn \rightarrow Et_3Sn^* + Et^*, \quad (5)$$

$$\equiv SnO_2 + Et_3Sn^* \rightarrow \equiv SnO_2 = SnEt_2 + Et^*, \quad (6)$$

$$\equiv SnO_2 = SnEt_2 \rightarrow = SnO_2 = Sn + {}_2Et^*, \quad (7)$$

$$\equiv SnO_2 = Sn + NO_2 \rightarrow \equiv SnO_2 = SnO_2 + NO. \quad (8)$$

We have carried out the experiments by obtaining stoichiometric SnO_2 using TET and H_2O_2 in the Resource Center “Innovative technologies of composite nanomaterials” SPbGU. According to XRR and elipsometric data, the growth rate was 0.2-0.3 Å/cycle. The amorphous films were obtained with the density of 6.4 g/cm^3. It should be noted that such value is rather high for amorphous films. The phase composition, rutile type SnO_2, was confirmed by XRD data for the annealed films.

4. CONCLUSION

The choice of the reactants is an important step in SnO_2 ALD procedure. The use of different precursors leads to various films properties. The metal-organic precursors have a considerable advantage because of their ability to diminish the synthesis temperature and to increase the growth rate and film purity. Among inorganic precursors, SnI_4 has great potential for the obtaining films with a uniform thickness, a flat surface, and a low defect density.

To obtain polycrystalline films, it is necessary to use the temperature higher than 250-300 °C or to carry out the additional stage of annealing after synthesis. It should be noted that the use of (Sn(tbba) and $Sn(dmamp)_2$) precursors decreases significantly the temperature of crystalline films formation (down to 120-130 °C). The selection of substrates for obtaining of heteroepitaxial films plays a very important role. TiO_2 single crystals, sapphire, and YSZ are usually used for these purposes.

The choice of oxidants is also one of the important requirements. In the case of TDMASn/H_2O_2 pair, the growth rate is reasonably high. Using of H_2O gives the possibility to obtain films at temperatures lower than 100 °C; this is important for production of thermally sensitive materials such as photovoltaic cells and organic light emitting diodes. The highest conductivity of films is observed in the case of O_3 usage, this conductivity is a very important factor for films application in TCOs.

ACKNOWLEDGMENTS

The reported study was supported by RFBR, research project № 14-03-31053 *mol_a and Program of megagrants of the Russian Ministry of Education and Science (Grant 14.B25.31.0017).*

REFERENCES

[1] M. Batzill and U. Diebold // *Progress in Surface Science* **79** (2005) 47.
[2] Z. Chen, D. Pan and Z. Li et al. // *Chem. Rev.* **114** (2014) 7442.
[3] S. Das and V. Jayaraman // *Progress in Materials Science* **66** (2014) 11.
[4] M.N. Rumyantseva, O.V. Safonova and M.N. Boulova // *Rus. Chem. Bull. Int. Ed.* **52** (2003) 1217.

[5] M.M. Arafat, B.Dinan and S.A. Akbar // *Sensors* **12** (2012) 7207.
[6] A. Rosental, A. Tarre and A. Gerst // *Sens. and Actuators B* **93**(2003) 552.
[7] G. Choi, L. Satyanarayana and J. Park // *Appl. Surf. Sci.* **252** (2006) 7878.
[8] D.H. Kim, W.-S.Kim and S.B. Lee // *Sens. Actuators B* **147** (2010) 653.
[9] N. Kamiuchi, T. Mitsui and N. Yamaguchi // *Journal of Catalysis* **184** (1999) 440.
[10] P.G. Harrison, C. Bailey and W. Azelee // *Catalysis Today* **157** (2010) 415.
[11] M.J. Fuller and M.E. Warwick // *Journal of Catalysis* **29** (1973) 441.
[12] T. Minami // *Semicond. Sci. Techno*l. **20** (2005) S35.
[13] R.G. Gordon // *MRS Bulletin* **25** (2000) 52.
[14] H. Liu, V. Avrutin and N. Izyumskaya // *Superlattices and Microstructures* **48** (2010) 458.
[15] D.S. Ginley and C. Bright // *MRS Bulletin* **25** (2000) 15.
[16] R.W. Jonson, A. Hultqvist and S.F. Bent // *Materials Today* **17** (2014) 236.
[17] R.E. Presley, C.L. Munsee and C-H. Park // *J. Phys. D: Appl. Phys.* **37** (2004) 2810.
[18] B.K. Lee, E. Jung and S.H. Kim // *Mat. Res. Bulletin* **47** (2012) 3052.
[19] D.-w. Choi, W.J. Maeng and J.-S. Park // *Appl. Surf. Sci.* **313** (2014) 585.
[20] S.-S. Tan, Y.-Y. Kee and H.-Y. Wong // *Surface & Coatings Technology* **231** (2013) 98.
[21] T.K. Yong, S.S. Yap and G. Sáfrán // *Applied Surface Science* **253** (2007) 4955.
[22] P. Görrn, F. Ghaffari and T. Riedl // *Solid-State Electronics* **53** (2009) 329.
[23] L-W. Chou, Y.-Y. Lin and A.T. Wu // *Applied Surface Science* **277** (2013) 30.
[24] B. Kang, L.W. Tan and S.R.P. Silva // *Appl. Phys. Lett.* **93** (2008) 133302.
[25] J. Lindahl, J.T. Wätjen and A. Hultqvist // *Prog. Photovolt: Res. Appl.* **21** (2013) 1588.
[26] M. Kapilashrami, C.X. Kronawitter and T. Törndahl // *Phys. Chem. Chem. Phys*. **14** (2012) 10154.
[27] R. Gordon // *Journal of Non-Crystalline Solids* **218** (1997) 81.
[28] C. Prasittichai and J.T. Hupp // *J. Phys. Chem. Lett*. **1**(2010)1611.
[29] X. Xu, F. Qiao and L. Dang // *J. Phys. Chem. C* **118** (2014) 16856.
[30] H.J. Snaith and C. Ducati // *NanoLett.* **10** (2010) 1259.
[31] S.F. Shaikh, R.S. Mane and O.-S. Joo // *RSC Adv.* **4** (2014) 35919.
[32] J.P.C. Baena and A.G. Agrios // *J. Phys. Chem. C* **118** (2014) 17028.
[33] J.S. Chen and X.W. Lou // *Small* **9** (2013) 1877.
[34] C.D. Lokhande, D.P. Dubal and O.-S. Joo // *Current Applied Physics* **11** (2011) 255.
[35] S.N. Pusawale, P.R. Deshmukh and C.D. Lokhande // *Applied Surface Science* **257** (2011) 9498.
[36] F. Grote, L. Wen and Y. Lei // *Journal of Power Sources* **256** (2014) 37.
[37] A.N. Subba Rao and V.T. Venkatarangaiah // *Environ. Sci. Pollut. Res.* **21** (2014) 3197.
[38] R.J. Watts, M.S. Wyeth and D.D. Finn // *J. Appl. Electrochem.* **38** (2008)31.
[39] L. Qin, T. Gong and H. Hao // *J. Nanopart. Res.* **15** (2013) 2150.
[40] J.D. Ferguson, K.J. Buechler and A.W. Weimer // *Powder Technology* **156** (2005) 154.
[41] C.B. Fitzgerald, M. Venkatesan and L.S. Dorneles // *Phys. Rev. B* **74** (2006) 115307.
[42] S.B. Ogale, R.J. Choudhary and J.P. Buban // *Phys. Rew. Lett*.**91** (2003) 077205-1
[43] R. Singh // *Journal of Magnetism and Magnetic Materials* **346** (2013) 58.
[44] T. Yu-Feng, H. Shu-Jun and Y. Shi-Shen // *Chin. Phys. B* **22** (2013) 088505.
[45] C. Van Komen, A. Thurber and K.M. Reddy // *J. Appl. Phys*. **103** (2008) 07D141.
[46] R.S. Hiratsuka, S.H. Pulcinelli and C.V. Santilli // *Journal of Non-Crystalline Solids* **121** (1990) 76.
[47] M. Ristić, M. Ivanda and S. Popović // *Journal of Non-Crystalline Solids* **303** (2002) 270.
[48] R.C. Singh, M.P. Singh and O. Singh // *Sensors and Actuators B* **143** (2009) 226.
[49] P.G. Mendes, M.L. Moreira and S.M. Tebcherani // *J. Nanopart. Res.***14** (2012) 750.
[50] U. Pal, M. Pal and R.S. Zeferino // *J. Nanopart.Res.***14** (2012) 969.
[51] W. Zeng, B. Miao and Q. Zhou // *Physica E* **47** (2013) 116.
[52] L. Tan, L. Wang and Y. Wang // *Journal of Nanomaterials* **2011** (2011) Article ID 529874.
[53] M. Samal and D.K. Yi // *Critical Reviews in Solid State and Materials Sciences* **38** (2013) 91.
[54] B.S. Thabethe, G.F. Malgas and D.E. Motaung // *Journal of Nanomaterials* **2013** (2013) Article ID 712361.

[55] S. Mathur and S. Barth // *Small* **3** (2007) 2070.
[56] M. Okuya, S. Kaneko and K. Hiroshima // *Journal of the European Ceramic Society* **21** (2001) 2099.
[57] G. Korotcenkov, V. Brinzari and V. Golovanov // *Sensors and Actuators B* **98** (2004) 41.
[58] S.G. Ansari, S.W. Gosavi and S.A. Gangal // *Journal of Materials Science: Materials in Electronics* **8** (1997) 23.
[59] F. Gu, S.F. Wang and M.K. Lu // *Journal of Crystal Growth* **262** (2004) 182.
[60] R.D. Sakhare, G.D. Khuspe and S.T. Navale // *Journal of Alloys and Compounds* **563** (2013) 300.
[61] G.D. Khuspe, R.D. Sakhare and S.T. Navale // *Ceramics International* **39** (2013) 8673.
[62] H. Sefardjella, B. Boudjema and A. Kabir // *Journal of Physics and Chemistry of Solids* **74** (2013) 1686.
[63] V.R. Katti, A.K. Debnath and K.P. Muthe // *Sensors and Actuators B* **96** (2003) 245.
[64] S. Bansal, D.K. Pandya and S.C. Kashyap // *Journal of Alloys and Compounds* **583** (2014) 186.
[65] M.S. Hu, B.S. Yan and J. Lee // *Thin Solid Films* **518** (2009) 1170.
[66] S. Min and J. Jeong // *Materials Science in Semiconductor Processing* **16** (2013) 1267.
[67] B. Wang, I.L. Li and P. Xu // *Rev. Adv. Mater. Sci.* **3** (2013) 164.
[68] M. Kwoka, N. Waczyńska and P. Kościelniak // *Thin Solid Films* **520** (2011) 913.
[69] C. Luan, Z. Zhu and W. M // *Vacuum* **99** (2014) 110.
[70] V.P. Tolstoy // *Russian Chemical Reviews* **75** (2006) 161.
[71] G. Korotcenkov, V. Tolstoy and J. Schwank // *Meas. Sci. Technol*. **17** (2006) 1861.
[72] H. Viirola and L. Niinistö // *Thin Solid Films* **249** (1994) 144.
[73] M. Utriainen, L. Niinistö and R. Matero// *Appl. Phys.A* **68** (1999) 339.
[74] M. Utriainen, K. Kovacs and J.M. Campbell // *J. Electrochem. Soc.* **146** (1999)189.
[75] C. Dücsö, N.Q. Khanh and Z. Horvath // *J. Electrochem. Soc.* **143** (1996) 683.
[76] S. Lehto, R. Lappalainen and H. Viirola // *Fresenius J. Anal. Chem*. **355** (1996) 129.
[77] M. Utriainen, H. Lattu and H. Viirola // *Mikrochim. Acta* **133** (2000) 119.
[78] H.-E. Cheng, D.C. Tian and K.-C. Huang // *Procedia Engineering* **36** (2012) 510.
[79] A. Tarre, A. Rosental and V. Sammelselg // *Appl. Surf. Sci*. **175/176** (2001) 111.
[80] A. Rosental, A. Tarre and A. Gerst // *Sens. and Actuators B* **77** (2001) 297.
[81] X. Du, Y. Du and S. M. George // *J. Vac. Sci. Technol. A* **23** (2005) 581.
[82] X. Du and S.M. George // *Sens. Actuators B* **135** (2008) 152.
[83] A. Tarre, A. Rosental and A. Aidla // *Vacuum* **67** (2002) 571.
[84] A. Tarre, A. Rosental and J. Sundqvist // *Surf. Sci.* **514** (2003) 532.
[85] J. Sundqvist, A. Tarre and A. Rosental // *Chem. Vap. Deposition* **9** (2003) 21.
[86] J. Lu, J. Sundqvist and M. Ottosson // *J. Cryst. Growth* **260** (2004) 191.
[87] A. Tarre, A. Rosental and T. Uustare // *Proceedings of SPIE - The International Society for Optical Engineering* **5946** (2005) 1.
[88] J.W. Elam, D.A. Baker and A.J. Hryn // *J. Vac. Sci. Technol. A* **26** (2008) 244.
[89] M.N. Mullings, C. Hägglund and S.F. Bent // *J. Vac. Sci. Technol. A* **31** (2013) 061503.
[90] J.T. Tanskanen and S.F. Bent // *J. Phys. Chem. C* **117** (2013) 19056.
[91] D. Choi and J.-S. Park // *Surf. Coat. Technol*. (2014) http://dx.doi.org/10.1016/j.surfcoat.2014.02.012
[92] D.H. Kim, J.-H. Kwon and M. Kim // *J. Cryst. Growth* **322** (2011) 33.
[93] S. Kim, D.-H. Kim and S.-H. Hong // *Journal of Crystal Growth* **348** (2012) 15.
[94] V. Aravindan, K.B. Jinesh and R.R. Prabhakar // *Nano Energy* **2** (2013) 720.
[95] J. Heo, A.S. Hock and R.G. Gordon // *Chem. Mater*. **22** (2010) 4964.
[96] J. Heo, S.B. Kim and R.G. Gordon // *J. Mater. Chem.* **22** (2012) 4599.
[97] S.K. Selvaray, A. Feinerman and C.G. Takoudis // *J. Vac. Sci. Technol. A* **32** (2014) 01A112.
[98] V.E. Drozd and V.B. Aleskovskii // *Appl. Surf. Sci.* **82/83** (1994) 591.
[99] M. Knez, K. Nielsch and L. Niinistö // *Adv. Mater.* **19** (2007) 3425.
[100] S.M. George // *Chem. Rev*. **110** (2010) 111.
[101] F. Zaera // *Coordination Chemistry Reviews* **257** (2013) 3177.
[102] R.L. Puurunen // *Journal of Applied Physics* **97** (2005) 121301.
[103] M.L. Huang, Y.C. Chang and C.H. Chang // *Appl. Phys. Lett.* **87** (2005) 252104.

[104] E.G. Zemtsova, A.Yu. Arbenin and A.F. Plotnikov // *J. Vac. Sci. Technol. A* **33** (2015) 021519.
[105] M.D. Groner, F.H. Fabreguette and J.W. Elam // *Chem. Mater.* **16** (2004) 639.
[106] A. Rahtu and M. Ritala // *Chem. Vap. Deposition* **8** (2002) 21.
[107] V. Pore, A. Rahtu and M. Leskelä // *Chem. Vap. Deposition* **10** (2004) 143.
[108] J. Aarik, A. Aidla and T. Uustare // *Journal of Crystal Growth* **148** (1995) 268.
[109] T. Tynell and M. Karppinen // *Semicond. Sci. Technol.* **29** (2014) 043001.
[110] A. Yamada, B. Sang and M. Konagai // *Applied Surface Science* **112** (1997) 216.
[111] P.F. Carcia, R.S. McLean and M.H. Reilly // *Appl. Phys. Lett.* **88** (2006) 123509.
[112] K. Kukli, M. Ritala and M. Leskelä // *Chem. Vap. Deposition* **6** (2000) 297.
[113] M. Cassir, F. Goubin and C. Bernay // *Applied Surface Science* **193** (2002) 120.
[114] S.-Y. Lee, H. Kim and P.C. McIntyre // *Appl. Phys. Lett.* **82** (2003) 2874.
[115] M. Putkonen, M. Bosund and O.M.E. Ylivaara // *Thin Solid Films* **558** (2014) 93.
[116] J.W. Klaus, O. Sneh and S.M. George // *Science* **278** (1997) 1934.
[117] J. Bachmann, R. Zierold and Y.T. Chong // *Angew. Chem. Int. Ed.* **47** (2008) 6177.
[118] P. Dagur, A.U. Mane and S.A. Shivashankar // *Journal of Crystal Growth* **275** (2005) 1223.
[119] O.M. Osmolowskaya and V.M. Smirnov // *Rev.Adv.Mater. Sci.* **27** (2011) 184.
[120] O.M. Osmolovskaya, I.V. Murin and V.M. Smirnov // *Rev.Adv.Mater. Sci.* **36** (2014) 70.
[121] D.V. Nazarov, O.M. Osmolovskaya and N.P. Bobrysheva // *Nanotechnologies in Russia* **7** (2012) 641.
[122] P. Sinsermsuksakul, J. Heo and W. Noh // *Adv. Energy Mater*. **1** (2011) 1116.
[123] L. Reijnen, B. Meester and A. Goossens // *Chem. Vap. Deposition* **9** (2003) 15.
[124] Y.S. Kim and S.J. Yun // *Applied Surface Science* **229** (2004) 105.
[125] J.A. van Delft, D. Garcia-Alonso and W.M.M. Kessels // *Semicond. Sci. Technol.* **27** (2012) 074002.
[126] V. Pore,T. Hatanpää and M. Ritala // *J. Am. Chem. Soc.* **131** (2009) 3478.
[127] J.S. Becker, S. Suh and S. Wang // *Chem. Mater.* **15** (2003) 2969.
[128] J.W. Elam, M. Schuisky and J.D. Ferguson // *Thin Solid Films* **436** (2003) 145.
[129] H. Kim // *J. Vac. Sci. Technol. B* **21** (2003) 2231.
[130] D.J.H. Emslie, P. Chadha and J.S. Price // *Coordination Chemistry Reviews* **257** (2013) 3282.
[131] H. Tiznado, M. Bouman and B.-C. Kang // *Journal of Molecular Catalysis A: Chemical* **281** (2008) 35.
[132] T.J. Knisley, L.C. Kalutarage and C.H. Winter // *Coordination Chemistry Reviews* **257** (2013) 3222.
[133] K.B. Ramos, M.J. Saly and Y.J. Chabal // *Coordination Chemistry Reviews* **257** (2013) 3271.
[134] M. Leskelä and M. Ritala // *Thin Solid Films* **409** (2002) 138.
[135] M. Leskelä and M. Ritala // *Angew. Chem. Int. Ed.* **42** (2003) 5548.
[136] V. Miikkulainen, M. Leskelä and M. Ritala // *J. Appl. Phys.* **113** (2013) 021301.
[137] J.S.Ponraj, G.Attolinia and M. Bosi // *Critical Reviews in Solid State and Materials Sciences* **38** (2013) 203.
[138] S.M. George, A.W. Ott and J.W. Klaus // *J. Phys. Chem.* **100** (1996) 13121.
[139] S.E. Potts and W.M.M. Kessels // *Coordination Chemistry Reviews* **257** (2013) 3254.
[140] L. Kong, J. Ma and Z. Zhu // *Journal of Crystal Growth* **312** (2010) 2931.
[141] L. Kong, J. Ma and Z. Zhu // *Materials Letters* **64** (2010) 1350.
L. Kong, J. Ma and C. Luan // *Applied Physics Letters* **98** (2011) 261904.